THE JOURNAL OF PHYSICAL CHEMISTRY C
Article
pubs.acs.org/JPCC

Permeation of a Single-Layer SiO_2 Membrane and Chemistry in Confined Space

Emre Emmez,[§] Bing Yang,[§] Shamil Shaikhutdinov,* and Hans-Joachim Freund

Abteilung Chemische Physik, Fritz-Haber Institute der Max-Planck Gesellschaft, Faradayweg 4-6, Berlin 14195, Germany

Supporting Information

ABSTRACT: Well-ordered, ultrathin silica films grown on metal substrates are composed of layers of corner-sharing $[SiO_4]$ tetrahedra (silicatene). Yet unrealized in practice as unsupported material, the double-layer silicatene could constitute the thinnest silica membrane ever fabricated. We addressed here the permeability of such a membrane by using a metal substrate as a gas detector. Permeation of CO and D_2 was examined by infrared reflection absorption spectroscopy and temperature-programmed desorption. The results reveal a complex response of such systems upon gas exposures which involves gas transport through amorphous silica pores as well as chemisorption and diffusion across the metal surface underneath the silicatene. Such a hybrid system, which would combine a robust molecular-sieve membrane and a chemically active metal underneath, could become interesting materials for technological applications, in particular, in catalysis and sensors.

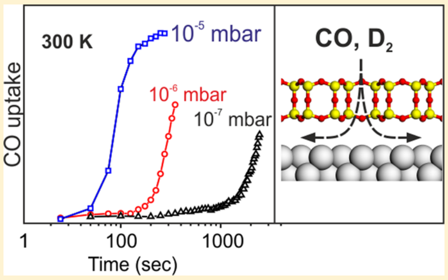

1. INTRODUCTION

Silicon dioxide (SiO_2) is a widely studied material because of its importance in geology, material science, microelectronics, photonics, and catalysis. Thin silica films are one of the key ingredients in many modern technological applications. Recent progress in fabrication of well-defined, ultrathin silica films on metal surfaces opened up opportunities for fundamental studies of silica-based materials at low dimensions.[1−4] The thinnest silica film forms a hexagonal layer of corner-sharing SiO_4 tetrahedra which is bound to a metal support through Si−O−Metal linkages[3] (henceforth referred to as silicatene). On noble metals such as Ru(0001) and Pt(111), a double-layer silicatene may be formed which is weakly bound to the support via dispersive forces (Figure 1a).[4−6] In contrast to a single-layer silicatene, the bilayer may exist in a crystalline and an amorphous (glassy) state in the layer (xy) plane, while maintaining highly ordered structure in the z-direction.[7−10] The amorphous silicatene exhibits a broad size distribution of N-membered rings that ranges from 4-membered to 9-membered rings, whereas the crystalline layer is composed exclusively of 6-membered rings. Both structures often coexist, showing smooth transformation from crystalline into the glassy state as shown in Figure 1b.

The "as prepared" silicatenes commonly contain oxygen atoms adsorbed directly onto the metal support.[4,11,12] The amount of oxygen underneath the silica is reduced upon annealing in ultrahigh vacuum (UHV), basically following the onset of O_2 desorption from the metal surface, and can be recovered by reoxidation.[11] In the case of the double-layer silicatene, the O coverage can be varied without structural changes of the silicatene itself. It appears that molecular oxygen may adsorb/desorb on/from the metal surface underneath the silica layer. In principle, the interlayer space between the silica sheet and the metal surface (which is computed to be in the range of 2.5−3 Å)[11] could be sufficient for surface diffusion of small adsorbed species and subsequent chemical reactions on the metal surface. It is therefore tempting to use the silica overlayer, which is essentially inert, as a molecular sieve for reactions that may otherwise occur unselectively on the supporting metal surface.

The permeation of single-layer silicatene, supported on Mo(112), has previously been examined both experimentally and theoretically with respect to metal (Au, Pd) atoms only.[13,14] Very recently, the group addressed adsorption of the same metal atoms on the bilayer silica as well.[15] The results show that Pd atoms penetrate through the silicatene and reach the metal support surface essentially without any barrier, while such a process considerably depends on ring size for Au adatoms.

In general, diffusion of gases in confined systems remains an interesting issue, in particular about whether a Knudsen description holds true when the pore size approaches the nanometer scale.[16−20] In this context, it is worth mentioning that a defect-free graphene membrane was found to be impermeable to standard gases, including helium.[21] However, theoretical calculations predicted extremely high selectivity to separate H_2 and CH_4 for graphene possessing defects as pores.[22] The principal structure of single-layer silicatene is essentially similar to that of graphene that would allow us to look into the properties of such truly two-dimensional systems solely on topology grounds.[23]

Special Issue: John C. Hemminger Festschrift

Received: April 2, 2014
Revised: May 21, 2014
Published: May 21, 2014

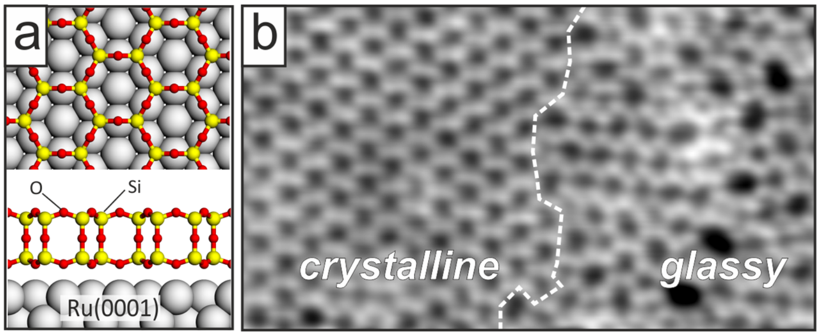

Figure 1. (a) Atomic structure of an ideal double-layer silicatene on Ru(0001). (b) STM image of coexisting crystalline and glassy (amorphous) structures of the silicatene.

In this work, we address the permeation of the double-layer silicatene (hereafter we skip "double-layer" for conciseness) with respect to simple gases, such as CO and D_2. Since silicatene cannot yet be fabricated as a free-standing sheet, the standard methods and techniques for mass transport studies cannot be applied. In attempts to elucidate the permeability of the silicatenes, we employ here a metal support (in this case Ru(0001)) as a gas detector, bearing in mind that the adsorption and coadsorption of O_2, CO, and H_2 on Ru(0001) is well-documented in the literature.[24−36] The results reveal a complex behavior which involves gas transport through the pores and diffusion across the metal surface underneath the silicatene. The results may aid in our understanding of the reactivity of such hybrid systems combining a molecular-sieve membrane and a chemically active metal underneath.

2. EXPERIMENTAL SECTION

The experiments were performed in an UHV chamber (base pressure $\sim 5 \times 10^{-10}$ mbar) equipped with a low-energy electron diffraction, infrared reflection−absorption spectroscopy (IRAS), and a quadrupole mass-spectrometer for temperature-programmed desorption (TPD) experiments. The IRA-spectra were recorded using p-polarized light at an 84° grazing angle of incidence (resolution 4 cm^{-1}). CO (purity grade 5.0), D_2 (3.0), and O_2 (6.0) were introduced into the chamber by using a cold trap to prevent contaminations.

The double-layer silicatene samples were grown on Ru(0001) as described in details elsewhere.[6] Briefly, silicon was vapor deposited onto oxygen precovered $3O(2 \times 2)$−Ru(0001) surface at ∼100 K, followed by oxidation at 1250 K in 10^{-6} mbar O_2. The quality of the films was inspected with IRAS (see Figure S1 in Supporting Information [SI]). Exposure to gases at pressures in the mbar range was performed in a separate cell sealed from the UHV chamber by a Viton O-ring. After the treatment, the cell was pumped out down to 10^{-7} mbar, and the sample was transferred back to the UHV chamber.

3. RESULTS

We first address the integrity of the silicatene samples and investigate whether they possess macroscopic "holes" which would certainly mislead the results on true gas permeation through the silica film. For this, we used CO as a probe molecule, as its interaction with the Ru surfaces, studied by both IRAS and TPD, is well documented in the literature. For quantitative analysis, we used a "Si-free" sample as a reference which is prepared under the same conditions as the silicatene sample, omitting solely the Si deposition step. Since CO chemisorbs on the clean and O/Ru surfaces with a high sticking coefficient at low temperatures, the "as prepared" silicatene samples were exposed to low CO pressures ($\sim 10^{-9}$ mbar) at 150 K. The simultaneously recorded IRA spectra revealed only a tiny peak at 2053 cm^{-1} (not shown here). The TPD spectrum from this sample is depicted in Figure 2a to compare with the spectra obtained on the clean Ru(0001) and Si-free samples. Clearly, the CO desorption profile from the silicatene sample resembles the one of the Si-free sample which is, in turn, very similar to those observed for CO on O-covered Ru(0001) surfaces.[35,37] The integral signal ratios indicate that the holes, if any, amount to a few percent of the whole sample surface area.

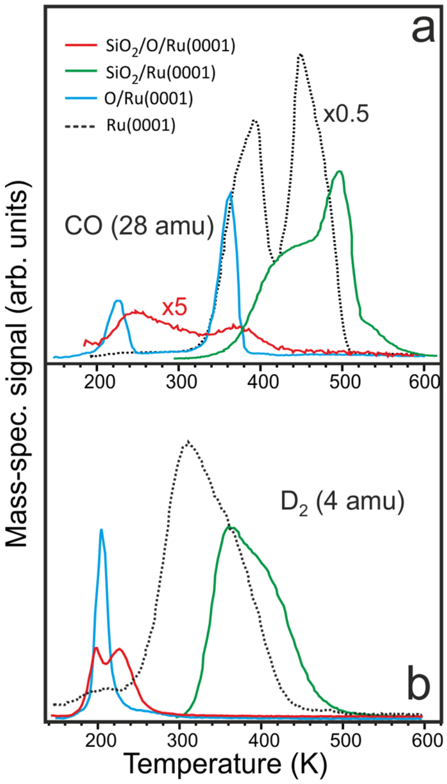

Figure 2. Comparison of TPD spectra of CO (a) and D_2 (b) from silicatene samples and clean and O-precovered Ru(0001) surfaces (see text for details).

Adsorption experiments with 10^{-6} mbar D_2 at 150 K on the "as prepared" samples did not show any D_2 desorption signal due to the well-known blocking effect of atomic oxygen on D_2 dissociation.[26,36] Therefore, in the next step, we address the preparation of the clean Ru(0001) surface underneath the silicatene; otherwise our "detector" will be silent toward the gases whose chemisorption is blocked by oxygen. In an attempt to desorb the O atoms from the Ru support, the samples were annealed at 1275 K for 1 min in UHV. This treatment strongly enhanced the D_2 uptake, while CO adsorption is affected only to a minor extent. The D_2 desorption profile featuring two peaks at 195 and 225 K (Figure 2b) differs considerably from that of the clean Ru(0001) surface and is similar to the one from the Si-free (O-covered) sample also shown in Figure 2b for comparison. The integral TPD area suggests that D atoms cover a substantial portion of the support for the annealed silicatene samples. Apparently, D_2 penetrates the silicatene easier than does CO. However, the annealed Ru surface underneath the silicatene remains to be covered by oxygen, albeit to a lower coverage as compared to the "as prepared" sample. Annealing for a longer time (up to 15 min) caused film dewetting, as evidenced by the attenuation of the principal phonon at 1300 cm^{-1} and concomitant growth of the broad band at ~1250 cm^{-1}, which is characteristic of bulk-like silica.[1,6]

In order to get rid of O species via its interaction with atomic D and subsequent desorption as water, the "as prepared" silicatene samples were exposed to higher pressures of D_2 (1 mbar) at 470 K and cooled down to 300 K before D_2 was pumped out. After this treatment, the principal 1300 cm^{-1} band in IRA spectra (not shown) is only slightly red-shifted, by a few wavenumbers, thus indicating that the silicatene structure is maintained. The TPD spectrum from such a sample (Figure 2b) is very similar to the spectrum of D_2 from the clean Ru(0001) surface, although the profile is shifted by ~40 K to higher temperatures and the intensity is reduced by ~33%. To see whether these effects are solely due to the high D_2 pressure used in this experiment, the sample was further exposed to 10^{-6} mbar D_2 at 300 K. Figure 3a displays a series of sequential TPD spectra at various exposure times. It appears that the D_2 uptake (i.e., integral desorption area at saturation) is almost independent of the pressure used (1 mbar vs 10^{-6} mbar). Moreover, the TPD spectra and the plots of integral desorption area vs exposure time are very similar to those observed for the clean Ru(0001) surface.[26] This implies that D_2 can easily reach the Ru(0001) surface at 10^{-6} mbar pressures even in the presence of the silicatene layer. If, however, the sample is exposed to D_2 at temperatures below 200 K, the D_2 uptake is considerably reduced (Figure 3b), whereas it is almost independent of the adsorption temperature (100−300 K) on the pristine Ru(0001) surface.[26,38] Since D_2 readily dissociates on Ru(0001) and the resulting D atoms easily diffuse across the surface at these temperatures,[30,33,39] the results indicate that the permeation of D_2 through the silicatene depends on temperature. However, the diffusion of D atoms on Ru may be affected by the silica layer as well. Therefore, to rationalize the TPD and IRAS results obtained upon exposure of metal−supported silicatene layers to various gases, one should take into account not only gas transport through the silicatene, but also adsorption (e.g., dissociation) and diffusion of adsorbed species on the metal surface.

Next we address CO adsorption on the silicatene having a clean Ru support underneath. In the next set of experiments, we exposed the sample to 2 × 10^{-6} mbar CO and simultaneously recorded IRA spectra. The measurements were first performed at a sample temperature of 100 K. Then CO was desorbed in front of a mass spectrometer in the TPD mode by heating to 700 K. The same experiment was then repeated at stepwise-increased sample temperatures, between 100 and 350 K. Figure 4 collects consecutive IRA spectra at indicated temperatures, reflecting the kinetics of CO adsorption on a metal support underneath the silicatene.

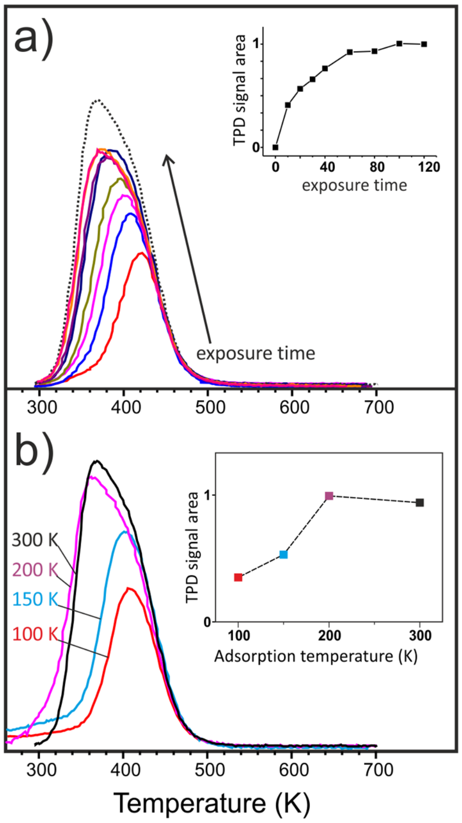

Figure 3. TPD spectra and TPD signal areas (in the insets) of 2 × 10^{-6} mbar D_2 adsorbed onto SiO_2/Ru(0001) as a function of exposure time (all exposures are at 300 K) (a) and temperature (all exposures are 2 min) (b). The dashed line in (a) shows the spectrum after exposure to 1 mbar D_2. TPD signal areas in the insets are normalized to the maximum.

At low temperatures (100−125 K, Figure 4a,b), the IR band peaking at 1931−1939 cm^{-1} (thereafter referred to as band I) saturates immediately, thus indicating a sticking coefficient of respective CO species as high as on the clean Ru(0001) surface. Then the band at ~2059 cm^{-1} (the band II) appears, that apparently saturates without any shift. For comparison, Figure S2 in the SI shows the series of IRA spectra recorded in a similar way over the clean Ru(0001) surface at 100 K, although exposed to a much lower pressure (10^{-8} mbar) in order to monitor spectral changes at increasing CO exposures. The signal appears first at ~1995 cm^{-1} and then continuously shifts to 2060 cm^{-1} upon increasing CO coverage until saturation, in good agreement with the previous results.[25]

Band II dominates the spectra at higher temperatures, as shown in Figure 4(a−g). The signal gains intensity and gradually shifts to 2055 cm^{-1} at 150 K, and further to 2051 cm^{-1} (200 K), 2044 cm^{-1} (250 K), 2037 cm^{-1} (300 K), and 2027 cm^{-1} (350 K), all measured after the same CO exposure (2 × 10^{-6} mbar, 2 min). Concomitantly, the low-frequency band I at 1939 cm^{-1}, which always appears first, strongly attenuates and vanishes at high exposures. The spectra at 250, 300, and 350 K revealed an additional band (band III) centered at ~2045 cm^{-1}, which might overlap with band II at low temperatures. The frequency of band III is almost independent

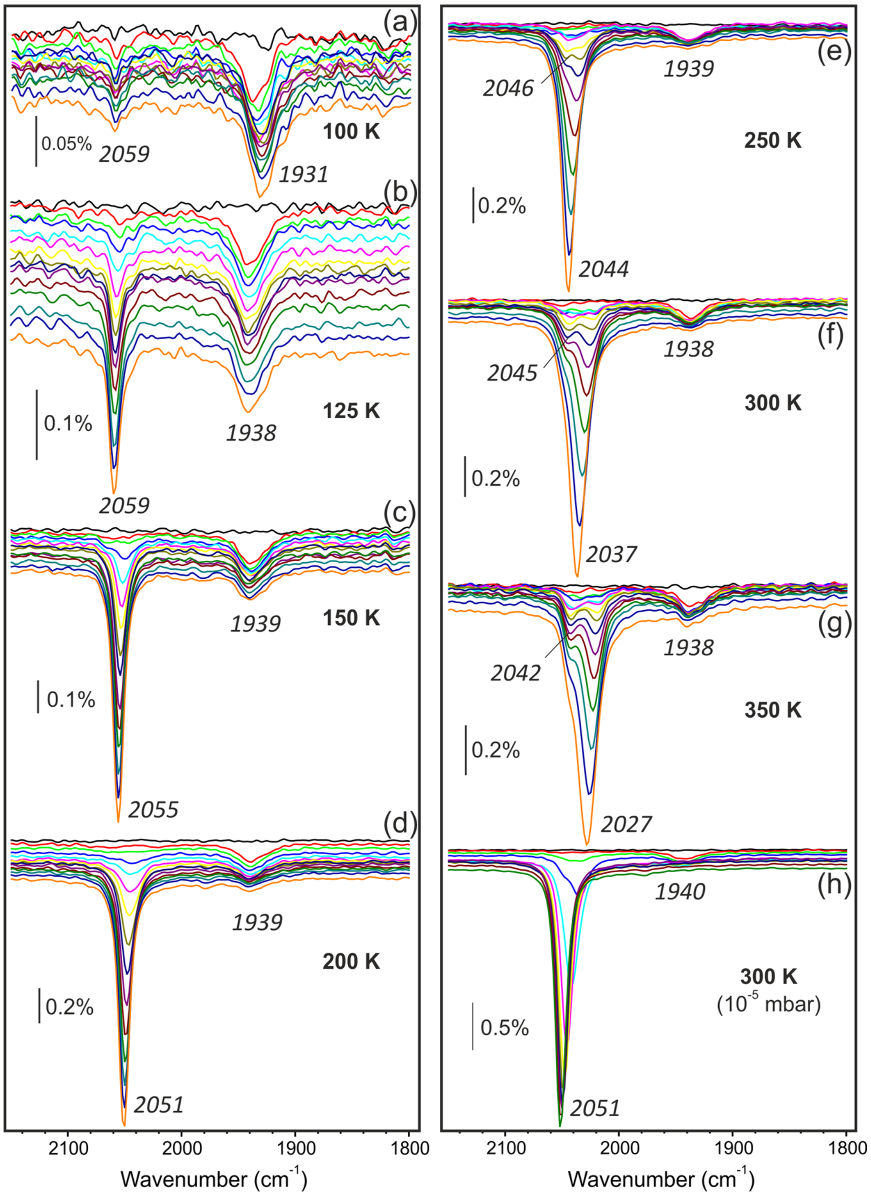

Figure 4. Consecutively recorded IRA spectra measured on SiO_2/Ru(0001) in 2 × 10^{-6} mbar CO (a–g) and 10^{-5} mbar CO (h) at the indicated temperatures. Each spectrum takes 12 s. The last shown spectrum corresponds to the 6-min exposure. Spectra are offset for clarity.

of adsorption temperature and exposure, whereas band II clearly shows the blue shift by about 5−10 cm^{-1} upon increasing CO coverage. It has turned out that at temperatures above 125 K saturation can hardly be achieved in 2 × 10^{-6} mbar of CO within reasonable time. To reach saturation, the experiments had to be performed at higher CO pressures, at least 10^{-5} mbar, as shown in Figure 4h. The spectrum at saturation shows only a very strong band II at 2051 cm^{-1}, i.e. at considerably higher frequency than 2037 cm^{-1}, observed in 2 × 10^{-6} mbar CO (both at 300 K; compare f and h of Figure4). This blue-shift agrees well with the coverage-dependent behavior observed on a clean Ru(0001) surface (Figure S3 in the SI).

In Figure 5a the final spectra from the plots presented in Figure 4(a−h) are compared. The corresponding TPD spectra recorded after the IRAS measurements are displayed in Figure 5b. First we note that the integral IRAS signal is proportional to the CO desorption signal (Figure 4c), both increase with adsorption temperature (inset in Figure 5b). We conclude that the IRA signal intensity is not affected by the CO adsorption geometry (CO axis is vertical or tilted with respect to the surface) due to the metal selection rules, but solely reflects CO surface population. In addition, this linear relationship (see Figure 5c) allows us to monitor the total CO coverage by IRAS.

As in the case of D_2 (see Figure 3b), the CO uptake increases in the temperature range from 100 to 200 K and then stays almost constant between 200 and 300 K. The desorption profile falls into the range of temperatures characteristic for CO desorption from a metallic Ru surface, but it is shifted by ~25 K (measured at the descending edge) toward higher temperatures, i.e. similarly to D_2 (Figure 2b). In addition, a prominent shoulder at the high-temperature side is seen, which is missing for the pristine Ru(0001) surface. Compared with pristine Ru(0001), the CO uptake over the silicatene-covered sample is reduced by ~38% (compare to ~33% observed for the D_2 uptake (Figure 2b)). As the CO saturation coverage on Ru(0001) is about 0.66 of monolayer (ML) (with respect to the number of the Ru surface atoms),[25,28] this yields

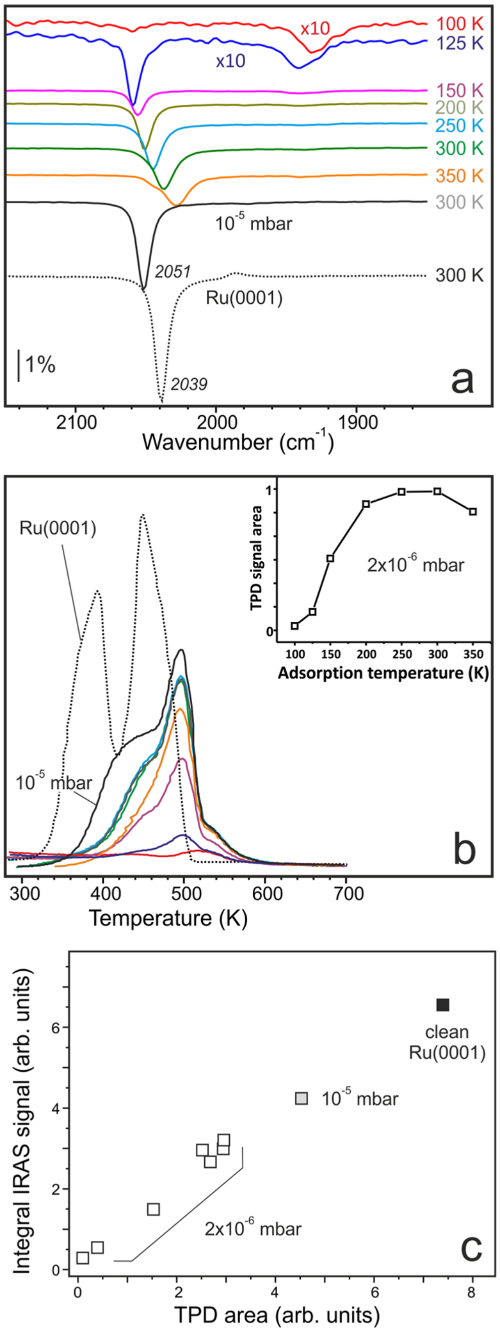

Figure 5. (a) The final IRA spectra taken from each plot (a–h) presented in Figure 4. (b) The corresponding TPD spectra of CO taken after the IRAS measurements. The inset shows the integral signal intensity as a function of adsorption temperature at 2×10^{-6} mbar CO. The results for the clean Ru(0001) surface are shown by the dotted line. The results for 10^{-5} mbar CO pressure are marked, for clarity. (c) Linear relation between all presented IRAS and TPD signals.

approximately 0.5 ML for the saturated CO coverage on Ru(0001) underneath the silicatene. Accordingly, we estimate 0.66 ML for the saturation D coverage underneath the silicatene using the saturation coverage of 1.0 ML for clean Ru(0001) as the reference.[26,30]

Since the vibrational bands related to the D atoms on Ru(0001) (relatively strong at 602 and weak at 833 cm^{-1})[29] could not be obtained with our spectrometer, the adsorption kinetics were analyzed by IRAS for CO adsorption only. Figure 6 displays the integral intensity of the each band (I, II, and III) as a function of exposure time at a specified temperature measured for the spectra depicted in Figure 4. Band I appears immediately with introducing CO, thus indicating that the respective CO species has the sticking coefficient as high as on the bare Ru(0001) surface. Moreover, its coverage is independent of adsorption temperature. Therefore, we have tentatively assigned those species to the "macroscopic holes" exposing clean Ru. However, the measured frequency (~1935 cm^{-1}) is much lower than ever detected on Ru(0001).[25] This implies that the vibrational properties of CO in such holes are strongly affected by the presence of the silica layer. CO adsorbing in two-fold (bridged) coordination, which commonly shows frequencies in this spectral region for many metals, albeit unusual for the Ru(0001) surface, would also be consistent with the shift. Nonetheless, the intensity of band I is indicative of a minority species and disappears at high CO coverage.

Apparently, the site corresponding to band III at ~2045 cm^{-1}, which can only be resolved at $T > 200$ K, populates the second, as more clearly seen in e–g of Figure 4. The frequency falls into the range typical for linear CO species on metallic Ru. Again, these species do not contribute much to the total CO uptake.

Clearly, band II dominates the spectra at high CO exposures and elevated temperatures. Figure 6 shows, however, that above 200 K the intensity of this band exhibits an induction period after which it steeply increases, ultimately approaching saturation (Figure 6h). The induction period strongly depends on CO pressure: the higher the pressure, the smaller the induction period, see Figure 7.

Finally, we note that upon adsorption of CO the silica phonon band at 1300 cm^{-1} is shifted toward higher frequencies by ~5 cm^{-1} (not shown). This behavior is very similar to that observed for the "O-rich" silicatene films having O directly adsorbed on the Ru support.[11] Accordingly, this shift is indicative of a further decoupling of the silicatene from the metal support because of the repulsive interaction between oxygens in the bottom layer of silicatene and CO.

4. DISCUSSION

The presented results reveal good integrity of the silicatene layer on a ~1 cm scale (diameter of the Ru single crystal), which allows us to neglect permeation of gases through macroscopic holes (on average) in order to rationalize the TPD and IRAS results. The key observations for CO and D_2 adsorption on the silicatene-covered Ru(0001) surface can be summarized as follows:

(i) Both D_2 and CO readily chemisorb on the Ru(0001) support underneath the silicatene layer, when exposed to 10^{-5}–10^{-6} mbar at temperatures above 200 K. The highest surface coverages, observed at these conditions, are ~0.5 ML for CO, and ~0.65 ML for D; both are about 35% lower than on the pristine Ru(0001) surface (Figure 2).

(ii) The CO and D_2 uptakes exhibit strong temperature dependence; both are considerably reduced at temperatures below 200 K, more notably for CO (Figures 3b and 5b).

(iii) When compared to the bare Ru(0001) surface, full desorption occurs at ~40 K (for D_2) and ~25 K (for CO) higher temperatures (Figure 2).

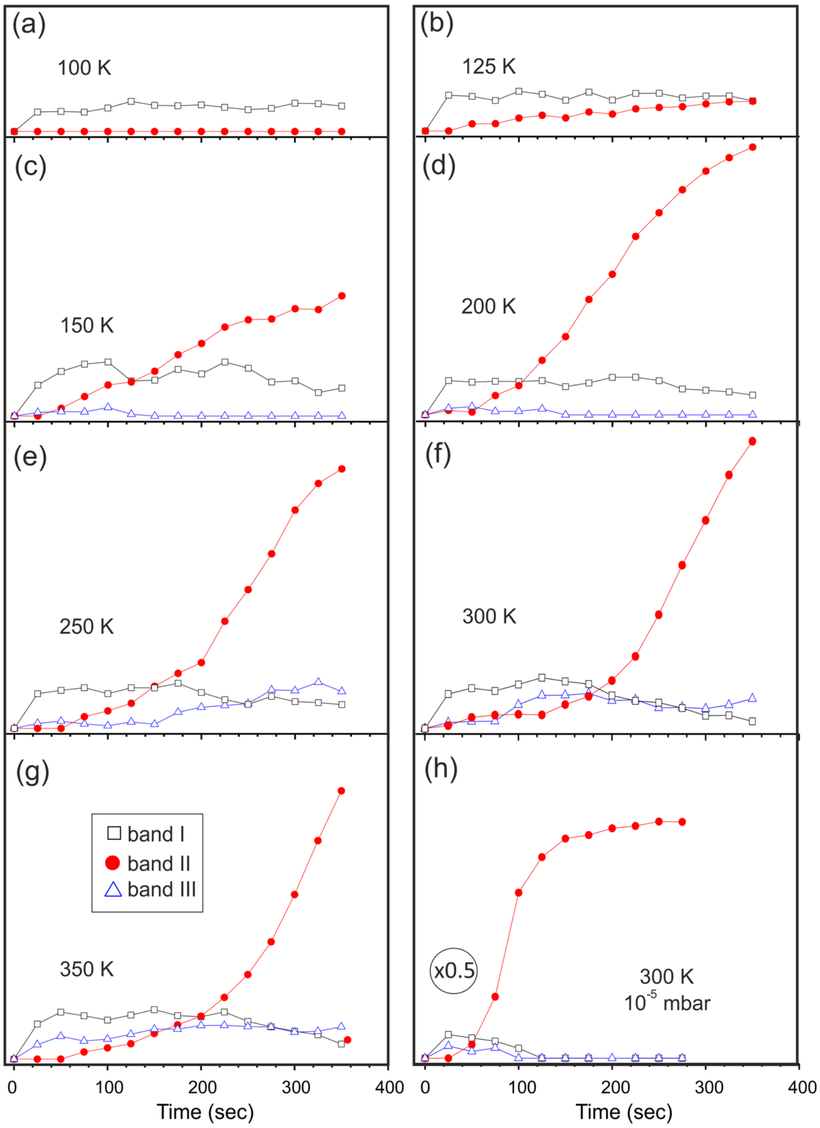

Figure 6. Kinetics of the IRA signal intensities of the each band (I, II, and III) obtained from the spectra presented in Figure 4

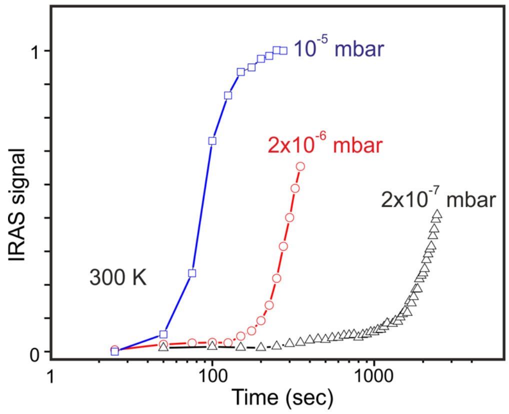

Figure 7. Kinetics of the CO uptake measured by IRAS at 300 K at three different CO pressures as indicated. Note the logarithmic scale for the exposure time.

(iv) In contrast to D_2, which shows a Langmuir-type adsorption kinetics (Figure 3a), CO adsorption at $T >$ 200 K exhibits an induction period followed by self-acceleration (Figure 6). The induction time decreases with increasing CO ambient pressure (Figure 7).

(v) CO adsorption reveals at least three CO surface species apparently having different sticking coefficients and fractional coverages.

Obviously, a general scenario upon exposure of the silicatene-covered Ru(0001) to the standard gases must involve the following steps: (1) penetration of a molecule through a pore in the silicatene; (2) adsorption on the metal surface right behind the pore; (3) diffusion of adsorbed species across the metal surface underneath the silica layer. Step (1) may include ballistic and nonballistic components, and may occur either through specific pores, associated with large N-membered rings, or uniformly. Step (2) may additionally include dissociation, as in the case of D_2. Furthermore, the adsorption site on the metal may be occupied by a previously adsorbed molecule (atoms) at low surface diffusion. In addition, all steps may be temperature dependent and have different rate constants.

At the temperatures studied here (100−300 K), hydrogen readily dissociates on the Ru surface.[26,29] Surface diffusion of hydrogen and deuterium on Ru(0001) at low coverage was studied earlier using laser-induced thermal desorption techniques.[31,32] In the temperature range between 260 and 330 K, the surface diffusion coefficient for deuterium was expressed in Arrhenius form as $D = 4.6 \times 10^{-4}$ cm^2/s exp(−4.1 (±0.5) kcal mol^{-1}/RT). Very recent studies, using helium spin−echo techniques and density functional theory (DFT) calculations, revealed tunneling−dominating fast diffusion at low temperatures (below 120 K) with the hopping rate of about 2×10^9 s^{-1}. Using the well-known formula for the diffusion length ($L = 2\sqrt{Dt}$), one can convince oneself that, at the time-scale of our experiments (typically, >10 s), the adsorbed D atoms diffuse very fast on Ru(0001), thus leading to a uniform D population across the surface, even at 100 K. Therefore, the temperature dependence observed for D_2 uptake must be assigned to a permeation step (1), assuming, of course, that D diffusion is not strongly affected by the silica layer.

CO diffusion on Ru(0001) is more complicated. Laser-induced thermal desorption measurements revealed a strong dependence of the diffusion coefficient on CO coverage.[40] For CO coverages below 0.3 ML, the coefficient measured at 290 K was approximately constant at $\sim 10^{-8}$ cm^2/s. As the CO coverage increased to 0.6 ML, the surface diffusion coefficient increased dramatically, up to 10^{-6} cm^2/s. At various temperatures (210−370 K) and CO coverages, the diffusivity displayed Arrhenius behavior. At 0.3 ML coverage, the diffusion coefficient is fitted by $D = 0.38$ cm^2/s exp(−11 kcal mol^{-1}/RT). At increasing CO coverage from 0.3 to 0.6 ML, both the activation energy and the pre-exponential factor decrease, i.e. from 11 to 6 kcal/mol, and from 0.38 to 0.06 cm^2/s, respectively. This was explained by the strong repulsive CO−CO interaction. Such complexity renders an estimation for the CO diffusion kinetics under our conditions rather difficult. Using the above values, one can estimate the diffusion length to be 10^3−10^4 nm at 300 K, but it becomes close or even smaller than the Ru(0001) lattice constant at 100 K. Therefore, at low temperatures, diffusion step (3) in CO adsorption experiments should, at least, be taken into account.

It has previously been established for the clean Ru(0001) surface, that the CO stretching frequency depends almost linearly on CO coverage (see ref 25 and also Figure S3 in the SI). In principle, such a relationship could be used for determining the CO coverage underneath the silicatene. However, comparing the IRA spectra, shown in Figure 5a, we see that the band, measured for the silica covered surface at 300 K, peaks at 2051 cm^{-1} at saturation, i.e. at a frequency much higher than 2039 cm^{-1} observed on pristine Ru(0001), although for a higher coverage in the latter case. The difference becomes even larger (∼17 cm^{-1}) if one compares spectra at equal, i.e. 0.5 ML, coverage (Figure S3 in the SI). Therefore, the stretching frequency of CO adsorbed on the Ru support is considerably higher in the presence of the silica layer above, although the frequency is blue-shifted at increasing CO exposure in the same way as on the pristine Ru (compare g and h of Figure 4 and Figure S3 in the SI). Assuming that the same difference holds true for adsorption at low temperatures, the band at 2059 cm^{-1} observed at 125 K for the silica sample would correspond to the coverage of about 0.4−0.5 ML, which would be almost an order of magnitude higher than the total CO coverage (0.05 ML) measured on this sample (Figure 5b,c). This finding can hardly be explained by CO penetrating uniformly. Indeed, if CO could penetrate through all cells in the honeycomb-like structure (see Figure 2a), ultimately resulting in one CO molecule per polygonal cell, one would expect to observe one IR band growing in intensity and blue-shifting with increasing CO exposure. This shift must be similar to that observed for pristine Ru(0001), i.e. ∼20−30 cm^{-1} (see Figure S3 in the SI). In fact, a−d of Figure 4 show that band III grows, in essence, without any shift. Apparently, CO molecules penetrate through specific pores and accumulate on the metal surface behind the pore to relatively high *local* concentration because of low surface diffusivity at low temperatures. At increasing temperature, the surface diffusion sets in, which diminishes the local CO concentration and thus causes the red-shift of the IRAS band, despite the total CO coverage increase, as shown in Figure 5. Certainly, the local concentration is determined by the flux of penetrating molecules and surface diffusivity. Within such a description, band III at ∼2045 cm^{-1} could tentatively be associated with CO species behind the pores at a quasi-steady state. At very high coverages, CO molecules become uniformly covering the whole Ru surface. As a result, bands I and III totally vanish.

Apparently, the CO desorption upon heating occurs through the same pores as the adsorption. Since the molecule needs some time to find these pores to escape, the desorption is delayed as compared with the pristine Ru(0001), thus resulting in the temperature shift in the TPD spectra (Figure 2). In the case of D_2, the desorption may delay even more, since it additionally includes D recombination to form D_2 which desorbs. Indeed, the observed shift for D_2 (∼40 K) is higher than for CO (∼25 K).

The conclusion about CO and D_2 penetration through specific pores is further supported by site blocking experiments. For this, the silicatene was first exposed to 10^{-6} mbar CO at 300 K for 1 min, resulting in a CO coverage of about 0.05 ML. Then 10^{-6} mbar D_2 was dosed to this surface at 300 K for 2 min. The TPD spectra with and without CO preadsorption are compared in Figure 8. Clearly, preadsorbed CO suppresses the D_2 uptake by a factor of ∼2. Although CO blocking of D_2 adsorption (dissociation) is well-documented in the literature for the Ru(0001) surface,[34,36] the total amounts of preadsorbed CO is too small to change the D_2 adsorption so drastically. Moreover, previous CO and D_2 coadsorption studies by TPD revealed a D_2 desorption temperature shift toward *low* temperatures, whereas in our experiments it shifts to *higher* temperatures. These findings can hardly be explained by uniform flux of D_2 molecules penetrating the silicatene and approaching the CO-precovered Ru surface. It seems more plausible that the D atoms, which reach the metal surface through those pores, exhibit limited surface diffusivity within

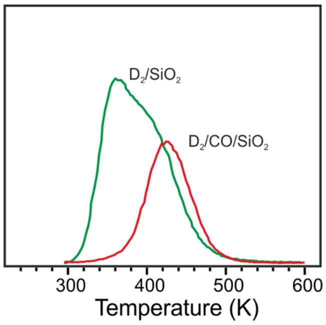

Figure 8. D_2 signals in TPD spectra of the silicatene after exposure to 2×10^{-6} mbar D_2 at 300 K for 2 min on the clean sample (green line) and the sample first exposed to 2×10^{-6} mbar CO at 300 K for 1 min (red line).

the precovered CO ad-layer. For the same reason, D_2 desorption is delayed in time during the TPD run, thus causing a further shift to higher temperatures in the TPD spectra (Figure 8).

The combined results indicate that a perfect crystalline silicatene is, in essence, impermeable for CO and D_2. The penetration of gas molecules occurs through the defects (pores) associated with larger than 6-member rings, commonly present in the amorphous silicatene. Since in all these experiments CO and D_2 ambient was kept at room temperature, the observed temperature dependence for CO and D_2 uptake (Figures 3b and 5b) cannot be explained by ballistic flow through the pores. In fact, Figure 5 shows that, at temperatures below 200 K, the CO uptake linearly grows in time, with the rate exhibiting Arrhenius behavior (see Figure S4 in the SI), yielding an apparent activation energy of 2.3 kcal/mol. This energy is remarkably lower than measured for CO diffusion on pristine Ru(0001) (between 6 and 11 kcal/mol).[40] Accordingly, the temperature dependence must be assigned to the activated penetration of CO through the silicatene pores rather than to the surface diffusion. Based on the kinetic diameters of D_2 and CO, which are about 2.9 and 3.8 Å, (although the numbers may deviate from those calculated by quantum mechanics[41]), the effective pore size allowing penetration would correspond to 8-membered rings as possible candidate.

The observation of an induction period for CO adsorption remains puzzling. As mentioned above, CO surface diffusivity on clean Ru(0001) exhibits nonlinear enhancement at increasing local CO coverage.[40] Therefore, it may well be that the increased local CO coverage right behind the pore, which is determined, basically, by the fluxes of penetrating molecules and those migrating away from the pore, both increasing with temperature, reached the situation when CO diffusivity strongly enhances due to the CO−CO repulsive interaction.[40] As an additional factor one may consider an increase of the distance between the silicatene and the metal surface which, in turn, favors further CO diffusion underneath the silica layer. In this respect, it is instructive here to address recent studies on intercalation of metal−supported graphene (refs 42−45 and references therein).

In particular, it was found that the Ru(0001) surface, fully covered by graphene, became passivated to O_2 adsorption at room temperature and only activated at elevated temperatures (>500 K). The adsorbed oxygen is intercalated between the graphene overlayer and the Ru(0001) surface and decouples the graphene layer from the substrate, forming a quasi-freestanding graphene layer floating on O/Ru(0001).[42] Oxygen intercalation competes with graphene etching that occurs at the domain edges and dominates at $T > 400$ °C.[43] It was further suggested that not only atomic O, formed by dissociation on the Ru surface surrounding the graphene domain, but even molecular O_2 diffuses between the graphene and the metal. Recent studies showed that also CO penetrates into the graphene/Pt(111) interface, but only through open channels at island edges at pressures $>10^{-6}$ mbar.[44] (No adsorption was observed for a fully covered graphene layer exposed to 10^{-6} mbar at 300 K for ca. 30 min.) Considering the kinetic diameter of CO (3.76 Å) and the distance between graphene and the Pt(111) substrate (3.30 Å),[43] it was concluded that CO intercalation enlarges the distance between the graphene sheet and the Pt surface as corroborated by DFT calculations, yielding the distance of about 5.9 Å.[44] The calculations also showed that CO adsorption on Pt(111) is weakened by the presence of the graphene above, in agreement with experimental results indicating that CO desorbs in UHV conditions even around room temperature. The earlier desorption of O atoms from the graphene/Ru(0001) interface rather than from the bare Ru(0001) surface was also reported previously.[42]

5. CONCLUSIONS

We studied CO and deuterium adsorption on double-layer silicatene films grown on Ru(0001) by infrared reflection absorption spectroscopy and temperature-programmed desorption. The results reveal a complex response of such systems upon gas exposures which involves gas transport through the pores (associated with structural defects in the silicatene), chemisorption, and diffusion across the metal surface underneath the silicatene. The results revealed some similarities as well as differences between the behavior of metal-supported silicatene and graphene with respect to the intercalation of molecules into the interface. Such a hybrid system, which would combine a robust molecular-sieve membrane and a chemically active metal underneath, could become an interesting material for technological applications, in particular, in catalysis and sensors.

■ ASSOCIATED CONTENT

Ⓢ Supporting Information

Typical IRA-spectrum of a double-layer silicatene film grown on Ru(0001), and IRA spectra of CO exposed to the clean Ru(0001) surfaces. This material is available free of charge via the Internet at http://pubs.acs.org.

■ AUTHOR INFORMATION

Corresponding Author

*E-mail: shaikhutdinov@fhi-berlin.mpg.de; Tel. +493084134114.

Author Contributions

§E.E. and B.Y. contributed equally.

Notes

The authors declare no competing financial interest.

■ ACKNOWLEDGMENTS

The work is supported by Deutsche Forschungsgemeinschaft through Collaborative Research Center SFB 1109. E.E. acknowledges International Max Planck Research School “Functional Interfaces in Physics and Chemistry” for the fellowship.

■ REFERENCES

(1) Shaikhutdinov, S.; Freund, H.-J. Ultrathin Silica Films on Metals: The Long and Winding Road to Understanding the Atomic Structure. *Adv. Mater.* **2013**, *25*, 49−67.

(2) Schroeder, T.; Adelt, M.; Richter, B.; Naschitzki, M.; Baumer, M.; Freund, H. J. Epitaxial Growth of SiO_2 on Mo(112). *Surf. Rev. Lett.* **2000**, *7*, 7−14.

(3) Weissenrieder, J.; Kaya, S.; Lu, J.-L.; Gao, H.-J.; Shaikhutdinov, S.; Freund, H.-J.; Sierka, M.; Todorova, T. K.; Sauer, J. Atomic Structure of a Thin Silica Film on a Mo(112) Substrate: A Two-Dimensional Network of SiO_4 Tetrahedra. *Phys. Rev. Lett.* **2005**, *95*, 076103.

(4) Löffler, D.; Uhlrich, J. J.; Baron, M.; Yang, B.; Yu, X.; Lichtenstein, L.; Heinke, L.; Büchner, C.; Heyde, M.; Shaikhutdinov, S.; Freund, H. J.; Włodarczyk, R.; Sierka, M.; Sauer, J. Growth and Structure of Crystalline Silica Sheet on Ru(0001). *Phys. Rev. Lett.* **2010**, *105*, 146104.

(5) Yu, X.; Yang, B.; Boscoboinik, J. A.; Shaikhutdinov, S.; Freund, H.-J. Support Effects on the Atomic Structure of Ultrathin Silica Films on Metals. *Appl. Phys. Lett.* **2012**, *100*, 151608.
(6) Yang, B.; Kaden, W. E.; Yu, X.; Boscoboinik, J. A.; Martynova, Y.; Lichtenstein, L.; Heyde, M.; Sterrer, M.; Wlodarczyk, R.; Sierka, M.; Sauer, J.; Shaikhutdinov, S.; Freund, H.-J. Thin Silica Films on Ru(0001): Monolayer, Bilayer and Three-dimensional Networks of [SiO_4] Tetrahedra. *Phys. Chem. Chem. Phys.* **2012**, *14*, 11344−11351.
(7) Lichtenstein, L.; Büchner, C.; Yang, B.; Shaikhutdinov, S.; Heyde, M.; Sierka, M.; Włodarczyk, R.; Sauer, J.; Freund, H.-J. The Atomic Structure of a Metal-Supported Vitreous Thin Silica Film. *Angew. Chem., Int. Ed.* **2012**, *51*, 404−407.
(8) Heyde, M.; Shaikhutdinov, S.; Freund, H. J. Two-Dimensional Silica: Crystalline and Vitreous. *Chem. Phys. Lett.* **2012**, *550*, 1−7.
(9) Lichtenstein, L.; Heyde, M.; Freund, H.-J. Atomic Arrangement in Two-Dimensional Silica: From Crystalline to Vitreous Structures. *J. Phys. Chem. C* **2012**, *116*, 20426−20432.
(10) Lichtenstein, L.; Heyde, M.; Freund, H.-J. Crystalline-Vitreous Interface in Two Dimensional Silica. *Phys. Rev. Lett.* **2012**, *109*, 106101.
(11) Włodarczyk, R.; Sierka, M.; Sauer, J.; Löffler, D.; Uhlrich, J. J.; Yu, X.; Yang, B.; Groot, I. M. N.; Shaikhutdinov, S.; Freund, H. J. Tuning the electronic structure of ultrathin crystalline silica films on Ru(0001). *Phys. Rev. B* **2012**, *85*, 085403.
(12) Todorova, T. K.; Sierka, M.; Sauer, J.; Kaya, S.; Weissenrieder, J.; Lu, J. L.; Gao, H. J.; Shaikhutdinov, S.; Freund, H. J. Atomic Structure of a Thin Silica Film on a Mo(112) Substrate: A Combined Experimental and Theoretical Study. *Phys. Rev. B* **2006**, *73*, 165414.
(13) Giordano, L.; Del Vitto, A.; Pacchioni, G. Au and Pd atoms Adsorbed on Pure and Ti-doped SiO_2/Mo(112) films. *J. Chem. Phys.* **2006**, *124*, 034701.
(14) Baron, M.; Stacchiola, D.; Ulrich, S.; Nilius, N.; Shaikhutdinov, S.; Freund, H. J.; Martinez, U.; Giordano, L.; Pacchioni, G. Adsorption of Au and Pd Atoms on Thin SiO_2 Films: The Role of Atomic Structure. *J. Phys. Chem. C* **2008**, *112*, 3405−3409.
(15) Kaden, W. E.; Büchner, C.; Lichtenstein, L.; Stuckenholz, S.; Ringleb, F.; Heyde, M.; Sterrer, M.; Freund, H.-J.; Giordano, L.; Pacchioni, G.; Nelin, C. J.; Bagus, P. S. Understanding Surface Core-Level Shifts Using the Auger Parameter: A Study of Pd Atoms Adsorbed on Ultrathin SiO_2 films. *Phys. Rev. B* **2014**, *89*, 115436.
(16) Holt, J. K.; Park, H. G.; Wang, Y.; Stadermann, M.; Artyukhin, A. B.; Grigoropoulos, C. P.; Noy, A.; Bakajin, O. Fast Mass Transport Through Sub-nanometer Carbon Nanotubes. *Science* **2006**, *312*, 1034−1037.
(17) Gruener, S.; Huber, P. Knudsen Diffusion in Silicon Nanochannels. *Phys. Rev. Lett.* **2008**, *100*, 064502.
(18) Kavalenka, M. N.; Striemer, C. C.; Fang, D. Z.; Gaborski, T. R.; McGrath, J. L.; Fauchet, P. M. Ballistic and Non-ballistic Gas Flow Through Ultrathin Nanopores. *Nanotechnology* **2012**, *23*, 145706.
(19) Unnikrishnan, S.; Jansen, H. V.; Falke, F. H.; Tas, N. R.; Wolferen, H. A. G. M. V.; Boer, M. J. D.; Sanders, R. G. P.; Elwenspoek, M. C. Transition Flow Through an Ultra-thin Nanosieve. *Nanotechnology* **2009**, *20*, 305304.
(20) Savard, M.; Tremblay-Darveau, C.; Gervais, G. Flow Conductance of a Single Nanohole. *Phys. Rev. Lett.* **2009**, *103*, 104502.
(21) Bunch, J. S.; Verbridge, S. S.; Alden, J. S.; van der Zande, A. M.; Parpia, J. M.; Craighead, H. G.; McEuen, P. L. Impermeable Atomic Membranes from Graphene Sheets. *Nano Lett.* **2008**, *8*, 2458−2462.
(22) Jiang, D.-e.; Cooper, V. R.; Dai, S. Porous Graphene as the Ultimate Membrane for Gas Separation. *Nano Lett.* **2009**, *9*, 4019−4024.
(23) Yang, B.; Boscoboinik, J. A.; Yu, X.; Shaikhutdinov, S.; Freund, H.-J. Patterned Defect Structures Predicted for Graphene Are Observed on Single-layer Silica Films. *Nano Lett.* **2013**, *13*, 4422−7.
(24) Pfnur, H.; Feulner, P.; Menzel, D. The Influence of Adsorbate Interactions on Kinetics and Equilibrium for CO on Ru(001). II. Desorption Kinetics and Equilibrium. *J. Chem. Phys.* **1983**, *79*, 4613−4623.
(25) Pfnür, H.; Menzel, D.; Hoffmann, F. M.; Ortega, A.; Bradshaw, A. M. High Resolution Vibrational Spectroscopy of CO on Ru(001): The Importance of Lateral Interactions. *Surf. Sci.* **1980**, *93*, 431−452.
(26) Feulner, P.; Menzel, D. The Adsorption of Hydrogen on Ruthenium (001): Adsorption States, Dipole Moments and Kinetics of Adsorption and Desorption. *Surf. Sci.* **1985**, *154*, 465−488.
(27) Kneitz, S.; Gemeinhardt, J.; Steinrück, H. P. A Molecular Beam Study of the Adsorption Dynamics of CO on Ru(0001), Cu(111) and a Pseudomorphic Cu Monolayer on Ru(0001). *Surf. Sci.* **1999**, *440*, 307−320.
(28) Pfnur, H.; Menzel, D. The Influence of Adsorbate Interactions on Kinetics and Equilibrium for CO on Ru(001). I. Adsorption Kinetics. *J. Chem. Phys.* **1983**, *79*, 2400−2410.
(29) Kostov, K. L.; Widdra, W.; Menzel, D. Hydrogen on Ru(001) Revisited: Vibrational Structure, Adsorption States, and Lateral Coupling. *Surf. Sci.* **2004**, *560*, 130−144.
(30) Lindroos, M.; Pfnür, H.; Feulner, P.; Menzel, D. A Study of the Adsorption Sites of Hydrogen on Ru(001) at Saturation Coverage by Electron Reflection. *Surf. Sci.* **1987**, *180*, 237−251.
(31) Mak, C. H.; Brand, J. L.; Deckert, A. A.; George, S. M. Surface Diffusion of Hydrogen on Ru(001) Studied Using Laser-Induced Thermal Desorption. *J. Chem. Phys.* **1986**, *85*, 1676−1680.
(32) Mak, C. H.; Brand, J. L.; Koehler, B. G.; George, S. M. Isotope Effect in the Surface Diffusion of Hydrogen and Deuterium on Ru(001). *Surf. Sci.* **1987**, *188*, 312−320.
(33) McIntosh, E. M.; Wikfeldt, K. T.; Ellis, J.; Michaelides, A.; Allison, W. Quantum Effects in the Diffusion of Hydrogen on Ru(0001). *J. Phys. Chem. Lett.* **2013**, *4*, 1565−1569.
(34) Peebles, D. E.; Schreifels, J. A.; White, J. M. The Interaction of Coadsorbed Hydrogen and Carbon Monoxide on Ru(001). *Surf. Sci.* **1982**, *116*, 117−134.
(35) Schiffer, A.; Jakob, P.; Menzel, D. The (2CO+O)(2 × 2)Ru(001) Layer: Preparation, Characterization, and Analysis of Interaction Effects in Vibrational Spectra. *Surf. Sci.* **1997**, *389*, 116−130.
(36) Ueta, H.; Groot, I. M. N.; Gleeson, M. A.; Stolte, S.; McBane, G. C.; Juurlink, L. B. F.; Kleyn, A. W. CO Blocking of D_2 Dissociative Adsorption on Ru(0001). *ChemPhysChem* **2008**, *9*, 2372−2378.
(37) Kostov, K. L.; Rauscher, H.; Menzel, D. Adsorption of CO on Oxygen-covered Ru(001). *Surf. Sci.* **1992**, *278*, 62−86.
(38) Shimizu, H.; Christmann, K.; Ertl, G. Model Studies on Bimetallic Cu/Ru catalysts: II. Adsorption of Hydrogen. *J. Catal.* **1980**, *61*, 412−429.
(39) Puisto, M.; Nenonen, H.; Puisto, A.; Alatalo, M. Effect of van der Waals Interactions on H_2 Dissociation on Clean and Defected Ru(0001) surface. *Eur. Phys. J. B* **2013**, *86*, 1−9.
(40) Deckert, A. A.; Brand, J. L.; Arena, M. V.; George, S. M. Surface Diffusion of Carbon Monoxide on Ru(001) Studied Using Laser-Induced Thermal Desorption. *Surf. Sci.* **1989**, *208*, 441−462.
(41) Mehio, N.; Dai, S.; Jiang, D.-e. Quantum Mechanical Basis for Kinetic Diameters of Small Gaseous Molecules. *J. Phys. Chem. A* **2014**, *118*, 1150−1154.
(42) Zhang, H.; Fu, Q.; Cui, Y.; Tan, D.; Bao, X. Growth Mechanism of Graphene on Ru(0001) and O_2 Adsorption on the Graphene/Ru(0001) Surface. *J. Phys. Chem. C* **2009**, *113*, 8296−8301.
(43) Sutter, P.; Sadowski, J. T.; Sutter, E. A. Chemistry under Cover: Tuning Metal−Graphene Interaction by Reactive Intercalation. *J. Am. Chem. Soc.* **2010**, *132*, 8175−8179.
(44) Mu, R.; Fu, Q.; Jin, L.; Yu, L.; Fang, G.; Tan, D.; Bao, X. Visualizing Chemical Reactions Confined under Graphene. *Angew. Chem., Int. Ed.* **2012**, *51*, 4856−4859.
(45) Feng, X.; Maier, S.; Salmeron, M. Water Splits Epitaxial Graphene and Intercalates. *J. Am. Chem. Soc.* **2012**, *134*, 5662.